

**PORE GEOMETRY AS A LIMITING FACTOR FOR ANION DIFFUSION IN
ARGILLACEOUS ROCKS**

C. Wigger^{1*}, M. Plötze², L.R. Van Loon³

¹Laboratory for Waste Management, Paul Scherrer Institut, 5232 Villigen PSI, Switzerland

²Institute for Geotechnical Engineering, 8093 Zurich, Switzerland

³Laboratory for Waste Management, Paul Scherrer Institut, 5232 Villigen PSI, Switzerland

Pre-publication

Corresponding author: Cornelia Wigger (cornelia.wigger@psi.ch)

Cornelia Wigger*

Paul Scherrer Institut

5232 Villigen PSI

Switzerland

cornelia.wigger@psi.ch

+41 56 310 5036

*corresponding author

article

Key Points

Bottleneck Effect, Opalinus Clay, Porosity, Retention Potential, Tortuosity

This document is the accepted manuscript version of the following article:
Wigger, C., Plötze, M., & Van Loon, L. R. (2018). Pore geometry as a limiting factor for anion diffusion in argillaceous rocks. *Clays and Clay Minerals*, 66(4), 329–338. <https://doi.org/10.1346/CCMN.2018.064101>



This is a 'pre-publication' version of an accepted article for *Clays and Clay Minerals*.

This version may be subject to change during the production process.

The DOI given, which may be used for citation purposes, though which will not be active until the version of record is published, is DOI: 10.1346/CCMN.2018.064101

ABSTRACT

1
2 Several barriers are foreseen to minimize the release of radionuclides from a waste matrix into
3 groundwater. In various countries argillaceous rocks constitute the natural barrier that will
4 isolate radioactive substances from the aquifer. This study addresses the influence of the pore
5 geometry as a limitation factor for anion diffusion in argillaceous rocks. Independent of the
6 pore core size the anion diffusion can be limited by the pore size opening, *i.e.* if the pore opening
7 is so narrow that the electric double layers overlap and form a barrier for anions independent of
8 the pore size. This bottleneck effect limits the anion diffusion. This study extends other
9 investigations that focus on different limitation factors of anion diffusion, *e.g.* mineralogy or
10 interlayer equivalent pores. The existence of so-called bottleneck pores was confirmed by
11 effective tortuosity calculations and retention potential measurements with mercury intrusion
12 porosimetry. On the basis of two different core samples from argillaceous rocks from
13 Switzerland, Opalinus Clay and Helvetic Marl, this work shows evidence for the existence of
14 bottleneck pores. The larger permanent anion exclusion in the Helvetic Marl sample compared
15 to the Opalinus Clay sample can be explained by the larger retention potential and larger
16 effective tortuosity of the Helvetic Marl rock, which indicates more pores with bottleneck
17 effects than for the Opalinus Clay rock.

18

19

20

21

22

INTRODUCTION

24 In various countries argillaceous rocks have been proposed as potential host rocks for deep
25 geological disposal of nuclear waste due to their favorable properties, such as self-sealing,
26 excellent sorption capacity for a wide range of radionuclides, and low hydraulic conductivity
27 restricting advective water flow towards the repository. Due to the low hydraulic conductivity,
28 molecular diffusion is the major transport process of radionuclides from the waste matrix
29 through the host rock towards the biosphere. Among the dose determining radionuclides,
30 anionic species such as ^{129}I , ^{36}Cl and ^{79}Se are the most important ones because their sorption on
31 rock minerals (in particular on the negatively charged clay minerals) is very weak or even zero
32 (Altmann, 2008; Grambow, 2008; Tournassat and Appelo, 2011). Understanding the behavior
33 of anions in clays and argillaceous rocks is thus very important to evaluate repository safety.
34 Several studies were performed to investigate the sorption and transport behavior of anions in
35 clays and clay rich materials such as bentonite (Appelt *et al.*, 1975; Bolt and de Haan, 1979;
36 Muurinen, 1994; Smith *et al.*, 2004; Van Loon *et al.*, 2007; Descostes *et al.*, 2008; Tournassat
37 and Appelo, 2011; Song *et al.*, 2016; Tournassat *et al.*, 2016a). The majority of the studies are
38 devoted to the determination of effective and apparent diffusion coefficients and capacity
39 factors for application in safety analyses of radioactive waste repositories. Neither the
40 differences of the results nor their origin are properly discussed in former studies; in particular
41 a proper experimental study of the pore characteristics influencing the anion diffusion in
42 argillaceous rocks is still open although some works can be found (Matuszewicz *et al.*, 2013;
43 Tournassat *et al.*, 2016b; Gaboreou *et al.*, 2016; Gimmi and Fernández, 2017).

44 Diffusion is mainly impacted by porosity, tortuosity and sorption, dictated by the density and
45 mineralogy of the argillaceous rocks. Unlike cations and neutral species, anions are partially
46 excluded from pores because of the permanent negative charge of clay mineral surfaces.
47 Moreover, the extent of anion exclusion depends on the ionic composition of the pore water. A

48 comparison study of different argillaceous rocks showed that the anion accessible porosity of
49 some argillaceous rocks is more dependent on the composition of the pore water than others
50 (Wigger and Van Loon, 2017). In the same study a permanent anion exclusion, *i.e.* a permanent
51 inaccessible pore space for anions independent on the ionic strength, was observed at an ionic
52 strength of the artificial pore water larger than 1 M NaCl. At the stage of 1 M NaCl the anion
53 accessible porosity values level off, and it can be expected that at this point the electrical double
54 layer is almost suppressed and increases less strongly with higher values of ionic strength. This
55 permanent exclusion value was different for the two compared clayrocks samples studied, *i.e.*
56 Opalinus Clay and Helvetic Marl. While Opalinus Clay sample has a comparatively small
57 permanent anion exclusion of 30% (as a fraction of the total porosity), Helvetic Marl sample
58 has a permanent anion exclusion of around 70%. The different values were explained by the
59 different mineralogy of the rocks (Table 1), and the presence of interlayer equivalent (ILE)
60 pores (Wigger and Van Loon, 2017). Interlayer equivalent pores are small pores in compacted
61 argillaceous rocks that are small enough to have – due to overlapping electric double layers –
62 similar properties as real interlayers, and are therefore inaccessible for anions. However,
63 although Helvetic Marl sample has a larger bulk dry density, and thus is more compacted with
64 lower total porosity than Opalinus Clay sample (Table 1), independent pore size distribution
65 (PSD) measurements indicated that the pores of Helvetic Marl sample were larger than those in
66 Opalinus Clay sample (Table 1), which means less but larger pores for the Helvetic Marl sample
67 (Houben *et al.*, 2013, Wigger *et al.*, 2018). The question why the permanent anion exclusion in
68 Helvetic Marl sample is larger than in Opalinus Clay samples, although the pores are larger in
69 size, remains an unresolved item. Therefore, the ILE theory needs to be revisited and the focus
70 has to be changed to another approach – the bottleneck pore theory-, as suggested by Wigger *et*
71 *al.*, 2018; as an alternative interpretation of permanent anion exclusion in argillaceous rocks
72 (Tournassat and Appelo, 2011). Similar to interlayer equivalent pores, bottleneck pores reduce
73 the anion accessible porosity independent of the pore size and independent of the ionic strength.

This is a 'pre-publication' version of an accepted article for Clays and Clay Minerals.

This version may be subject to change during the production process.

The DOI given, which may be used for citation purposes, though which will not be active until the version of record is published, is DOI: 10.1346/CCMN.2018.064101

74 Not the whole pore space needs to be narrow like in ILE pores in order to cause overlapping
75 electric double layers. In the case of bottleneck pores only the pore openings are narrow
76 (< 0.5 nm) and the electric double layer is overlapping at the pore throat and hinders the anion
77 transport in argillaceous rocks (Figure 1). This fact does not change significantly with
78 increasing ionic strength and leads to a permanent anion exclusion in these pores (Tournassat
79 and Appelo, 2011, Chagneau *et al.*, 2015).

80 Hence, the diffusion data published in Wigger and Van Loon (2017) was used and performed
81 a more detailed mercury intrusion porosimetry study on the same samples used in Wigger and
82 Van Loon (2017) to collect more information on the pore structure of the argillaceous rocks.
83 The presented study focuses on the anion diffusion limited by the connectivity of pores caused
84 by so-called bottleneck pores based on tortuosity calculations and retention potential
85 measurements.

87 **Samples**

88 The rock samples used for this study are the same samples used in an earlier study (see Wigger
89 and Van Loon, 2017): an Opalinus Clay core sample from a deep borehole (SLA-1) in
90 Schlattingen (Canton of Thurgau, Switzerland) at a depth of -936.25 m below surface; and a
91 Helvetic Marl core sample from a deep borehole (WLB SB4a/v) in Wellenberg (Canton of
92 Nidwalden, Switzerland) at a depth of -474.86 m below surface. Schlattingen and Wellenberg
93 have been proposed as suitable regions for hosting a repository for high-level (HLW) and low-
94 and intermediate-level (L/ILW) waste, respectively, in Switzerland. The differences of these
95 two samples are interesting for a comparative study. Additionally, it is attractive that a lot of
96 studies were already performed with these two samples and these work is therefore based on a
97 proper database. The mineral composition of the rocks and the most important physical
98 parameters are summarized in Table 1.

99 **Tortuosity calculation**

100 The diffusion of anions in argillaceous rocks is influenced by the mineralogy and the pore
101 network geometry of the sample. The diffusion coefficients of HTO and $^{36}\text{Cl}^-$ were measured
102 in a former study (Wigger and Van Loon, 2017), and were used in this study for novel
103 calculations of the geometric factors.

104 According to Fick's first law, the mass of a diffusing substance passing through a given cross-
105 section per unit time is proportional to the concentration gradient, and – for a one dimensional
106 case – is defined as:

$$107 \quad J = -D \cdot \frac{\partial C}{\partial x} \quad (1)$$

108 where, J is the mass flux density [$\text{mol}\cdot\text{m}^{-2}\cdot\text{s}^{-1}$], D is the diffusion coefficient [$\text{m}^2\cdot\text{s}^{-1}$], C is the
109 species concentration [$\text{mol}\cdot\text{m}^{-3}$] and $\frac{\partial C}{\partial x}$ is the concentration gradient [$\text{mol}\cdot\text{m}^{-4}$] (Harvey, 1996).

110 If the concentration within the system is changing with space and time [s], Fick's second law
111 applies:

$$112 \quad \frac{\partial C}{\partial t} = D_a \cdot \frac{\partial^2 C}{\partial x^2} \quad (2)$$

113 with,

$$114 \quad D_a = \frac{D}{\alpha} \quad , \quad (3)$$

115 where, D_a is the apparent diffusion coefficient and the rock capacity factor α is defined as:

$$116 \quad \alpha = \eta_t + \rho \cdot K_d \quad (4)$$

117 where, K_d represents the equilibrium distribution coefficient [$\text{m}^3\cdot\text{kg}^{-1}$] and ρ is the dry bulk
118 density of the rock [$\text{kg}\cdot\text{m}^{-3}$]. For non-sorbing tracers, such as anions, $K_d = 0$, and the rock
119 capacity factor α equals the transport porosity η_t (Van Loon and Soler, 2004).

120 It is necessary to modify Fick's law for the evaluation of the diffusion through a fluid in a two
121 phase system, such as water in a porous rock. The modification is applied by redefining the
122 diffusion coefficient, D , to the effective diffusion coefficient, D_e , including factors such as the
123 porosity and the pore geometry, which is defined by a combination of tortuosity and
124 constrictivity (Vilks and Miller, 2007).

125 The effective diffusion coefficient, D_e , is a kind of mass conductivity and commonly used to
126 describe diffusive fluxes in porous media and is related to the diffusion coefficient in the pore
127 solution, D_{ps} [$\text{m}^2\cdot\text{s}^{-1}$] by:

$$128 \quad D_e = \frac{\eta_t \cdot \delta}{\tau^2} \cdot D_{ps} \quad , \quad (5)$$

129 where, η_t is the transport porosity of the solid phase in which the diffusion takes place, δ is
130 the constrictivity and accounts for the fact that the pore diameter varies along the pathway [-],
131 and τ is the tortuosity of the sample and takes account for path lengthening [-] (Choi and
132 Oscarson, 1996; Tevissen *et al.*, 2004; Van Brakel and Heertjes, 1974).

133 The constrictivity, δ , and tortuosity, τ , are difficult or even impossible to determine separately
134 (Vilks and Miller, 2007). Because of the difficulty in separating δ and τ , the term effective
135 tortuosity was introduced by Melnyk and Skeet (1986) and Katsube *et al.* (1986), and is defined
136 as:

$$137 \tau_D^2 = \frac{\tau^2}{\delta} . \quad (6)$$

138 The effective tortuosity values can be calculated by combining equation 5 and 6:

$$139 \tau_D^2 = \frac{\tau^2}{\delta} = \frac{\eta_t \cdot D_{ps}}{D_e} \quad (7)$$

140 from measured values of effective diffusion coefficients, computed porosity values from bulk
141 and grain density (assumed that $\eta_t \approx \eta_{tot}$), and diffusion coefficients in pore solution
142 calculated by Stokes-Einstein equation:

$$143 D_{ps} = \frac{k_B \cdot T}{6 \cdot \pi \cdot \vartheta \cdot r} , \quad (8)$$

144 where, k_B is the Boltzmann constant [$\text{J} \cdot \text{K}^{-1}$], T is the temperature [K], ϑ is the dynamic viscosity
145 of the pore water solution [$\text{N} \cdot \text{s} \cdot \text{m}^{-2}$] and r is the hydrodynamic radius of the diffusing species
146 [m].

147 **Mercury intrusion porosimetry**

148 In this study, the existence of so-called bottleneck pores was experimentally evaluated by
149 mercury intrusion porosimetry (MIP). The idea is based on the study of Wardlaw and McKellar
150 (1981), who described pore systems that affect the trapping of non-wetting fluids, such as
151 mercury, after pressure reduction, and discussed how the shape of the mercury injection and
152 withdrawal curves are affected by the geometry of the pores and their connectivity.

153 In a first step, the clay samples have been analyzed by MIP using a Pascal 140 + 440 mercury
154 intrusion porosimeter (Thermo Scientific™, Germany) for measuring macro- and mesopores
155 with a radius in the range of 1.8 – 58000 nm. Samples of approximately 3 – 5 g were used. For
156 avoiding erroneous measurements caused by residual water in the sample, the argillaceous
157 rocks have been crushed into small pieces (< 500 mm³), then shock frozen with liquid N₂ and
158 finally applied to vacuum overnight to dry the sample as gently and efficiently as possible,
159 avoiding changes in the pore geometry, *e.g.* avoid shrinking (Thompson *et al.*, 1985).

160 The MIP measurements were conducted by increasing the pressure up to 400 MPa on a rock
161 sample immersed in the non-wetting mercury. Thus, the rate of pressure increment was
162 controlled automatically and adjusted in a progressed procedure with lower rates at lower
163 pressure levels and during measured intrusion processes. Mercury enters smaller voids
164 incrementally with increasing pressure. The pore volume can be deduced from the amount of
165 intruded mercury. The pore size is determined as a function of external pressure, which is
166 necessary to force the liquid into a pore against the surface tension of the liquid. The calculation
167 of the pore size distribution is based on the Washburn-equation (Washburn, 1921a; Washburn
168 1921b):

$$169 \quad r_{pore} = \frac{2\gamma \cos\theta}{\Delta P} \quad (9)$$

170 where, r_{pore} is the pore throat radius, γ the surface tension of mercury ($\gamma \approx 0.48 \text{ N}\cdot\text{m}^{-1}$), θ the
171 contact angle between the solid and mercury ($\theta = 147^\circ$) and ΔP is the pressure gradient applied
172 (Diamond, 1970; Giesche, 2006). From the first intrusion measurement the porosity can be
173 calculated from the total injected mercury volume, as well as the pore size distribution of the
174 sample as a function of the external pressure. In a second step, the pressure is reduced until
175 atmospheric pressure. Because of the pressure reduction, a withdrawal process will take place
176 and the mercury will be released. This withdrawal process is equally measured and logged as
177 the intrusion process. The intrusion curve plots the volume change caused by increasing

This is a 'pre-publication' version of an accepted article for Clays and Clay Minerals.

This version may be subject to change during the production process.

The DOI given, which may be used for citation purposes, though which will not be active until the version of record is published, is DOI: 10.1346/CCMN.2018.064101

178 pressure, while the extrusion curve represents the volume change with decreasing pressure. It
179 can be concluded that some mercury has been permanently entrapped in the sample pore space,
180 when the intrusion-extrusion cycle does not close when the incipient pressure is reached. The
181 amount of the entrapped mercury can be evaluated by the difference between the intrusion and
182 extrusion curves (Moro and Böhni, 2002). Such a hysteresis indicates the presence of bottleneck
183 pores. The larger the hysteresis, the larger the retention potential of the sample and the more
184 bottleneck-type pores might be expected in the sample.

185 After a first intrusion-extrusion cycle, a second intrusion measurement was started. Due to the
186 fact that mercury from the first cycle remained trapped in the bottleneck pores, only the empty
187 non-bottleneck pores become refilled in the second measurement and enable detection of the
188 pore volume of the non-bottleneck pores.

189 The withdrawal efficiency (W_e) is the ratio, expressed as a percentage, of the volume of mercury
190 withdrawn, V_w , from the sample at minimum pressure (101.325 kPa) to the volume injected
191 before pressure was reduced, *i.e.* the total volume, V_{tot} :

$$192 \quad W_e = \frac{V_w \cdot 100}{V_{tot}} \quad (10)$$

193 In this study the total volume, V_{tot} , is related to the total porosity, η_{tot} , of the sample, while the
194 volume of withdrawn mercury, V_w , equals the volume of the pores with a low pore to throat size
195 ratio, η_w . The volume data is corrected to the compressibility and temperature-dependent
196 volume of mercury.

197

199 **Tortuosity calculations based on diffusion experiments**

200 The effective tortuosity calculations were performed as described in the Materials and Method
 201 Section by equation 7. The transport porosity, η_t , as well as the effective diffusion coefficient,
 202 D_e , were known from previous experimental studies described in Wigger and Van Loon (2017).
 203 For an ionic strength of the pore solution of 1 M NaCl, the effective diffusion coefficient of
 204 HTO in the Opalinus Clay sample is $1.12 \cdot 10^{-11} \text{ m}^2/\text{s}$ and that of $^{36}\text{Cl}^-$ is $2.25 \cdot 10^{-12} \text{ m}^2/\text{s}$. The
 205 transport porosity of HTO equals 11.4%, whereas the anion transport porosity measured by
 206 $^{36}\text{Cl}^-$ diffusion is 6.9% in the Opalinus Clay sample. The values are larger than the ones for the
 207 Helvetic Marl sample, where the effective diffusion coefficient of HTO is $1.06 \cdot 10^{-12} \text{ m}^2/\text{s}$ and
 208 $1.22 \cdot 10^{-13} \text{ m}^2/\text{s}$ for $^{36}\text{Cl}^-$. The transport porosity of HTO in the Helvetic Marl sample is 3% and
 209 that of $^{36}\text{Cl}^-$ equals 0.85%.

210 For calculation of the diffusion coefficients in the solution D_{ps} , the already known parameters
 211 ϑ_{ps} , ϑ_w and D_w were needed (equation 12):

$$212 \quad D_{ps} \cdot \vartheta_{ps} = \frac{k_B \cdot T}{6 \cdot \pi \cdot r} = D_w \cdot \vartheta_w \quad , \quad (11)$$

$$213 \quad D_{ps} = \frac{D_w \cdot \vartheta_w}{\vartheta_{ps}} \quad , \quad (12)$$

214 where, k_B is the Boltzmann constant ($1.38 \cdot 10^{-23} \text{ J} \cdot \text{K}^{-1}$), T is the temperature (298.15 K), ϑ_{ps} is
 215 the dynamic viscosity of 1 M NaCl pore solution ($9.72 \cdot 10^{-4} \text{ N} \cdot \text{s} \cdot \text{m}^{-2}$ (Kestin *et al.* 1981)) ϑ_w is
 216 the dynamic viscosity of pure water ($8.91 \cdot 10^{-4} \text{ N} \cdot \text{s} \cdot \text{m}^{-2}$) and D_w is the diffusion coefficient of
 217 HTO in water ($2.00 \cdot 10^{-9} \text{ m}^2 \cdot \text{s}^{-1}$) and for chloride in pure water ($2.032 \cdot 10^{-9} \text{ m}^2 \cdot \text{s}^{-1}$ (Flury and
 218 Gimmi, 2002)), r is the hydrodynamic radius for water $1.38 \cdot 10^{-10} \text{ m}$ and for chloride $1.21 \cdot 10^{-10}$
 219 m.

220 This results in a pore solution diffusion coefficient, D_{ps} , of about $1.85 \cdot 10^{-9} \text{ m}^2/\text{s}$ for both HTO
221 and $^{36}\text{Cl}^-$.

222 Based on equation 7, the effective tortuosity, τ_D^2 , could be calculated. The results are
223 summarized in Table 2.

224 **Hg-retention potential measurements**

225 Figure 2 shows the cumulative pore volume (mm^3/g) for the intrusion (solid line) and extrusion
226 (dashed line) process during a mercury intrusion-extrusion cycle for Opalinus Clay and Helvetic
227 Marl rock samples. A significant hysteresis is observable for both samples. Furthermore, the
228 extrusion curve stops before the initial pressure is reached, *i.e.* both samples do not have a
229 continuous mercury path towards the sample surface and pores remained filled with mercury.

230 Mercury intrusion measurements show a porosity of $29.6 \text{ mm}^3/\text{g}$ for Opalinus Clay sample and
231 $6.9 \text{ mm}^3/\text{g}$ for Helvetic Marl sample (Table 3). Analysis from the withdrawal data gives a
232 trapped mercury volume of $18.8 \text{ mm}^3/\text{g}$ for the Opalinus Clay sample and a trapped mercury
233 volume of $6.3 \text{ mm}^3/\text{g}$ for the Helvetic Marl sample. That means that Opalinus Clay sample has
234 a withdrawal efficiency, W_e , of 36.4% and Helvetic Marl sample has only a W_e of 9.1%. This
235 would mean that the Helvetic Marl sample has a much larger Hg-retention potential than
236 Opalinus Clay. However, it needs to be considered that the device stops measuring before
237 atmospheric pressure is reached, hence the total withdrawal potential cannot be read out from
238 the first measurement run. Therefore, the device was opened after the first run to ensure that
239 the atmospheric pressure was reached and all mercury with withdrawal potential withdraws
240 until the threshold (atmospheric pressure) is reached.

241 After the first intrusion-extrusion cycle, a second measurement run was started. In this case
242 only the withdrawn pores will filled again. The total volume measured during the second
243 measurement thus corresponds to the withdrawal volume from the first measurement. In the

244 case of Opalinus Clay sample $11.43 \text{ mm}^3/\text{g}$ could be withdrawn, whereas for Helvetic Marl
245 sample the withdrawn volume is $1.61 \text{ mm}^3/\text{g}$. As recognizable in Table 3, the total withdrawal
246 volume, which is defined as the total volume in the second run, the retention potential of
247 Opalinus Clay sample equals 61% ($100\% - 39\%$) and that of Helvetic Marl sample 77% (100%
248 $- 23\%$).

249 The withdrawal volume in the second run should be 100% if the pressure could be decreased to
250 the atmospheric pressure. However, this is not the case. As long as the apparatus is running,
251 there is always a remaining pressure which is larger than the atmospheric pressure.

252

253

DISCUSSION

254 **Tortuosity analysis**

255 The effective tortuosity for HTO and $^{36}\text{Cl}^-$ is a function of the ionic strength of the pore solution
256 (Figure 3). In the case of HTO, the effective tortuosity has a constant value of 17.8 ± 1.9 for
257 Opalinus Clay sample or 33.3 ± 4 for Helvetic Marl sample, and does not depend on the
258 composition of the pore solution. From this information, and also from the fact that the HTO
259 effective porosity is independent of the composition of the pore solution, it can be concluded
260 that HTO is not affected by any electrical effect. Unlike HTO, in the case of $^{36}\text{Cl}^-$, the effective
261 tortuosity clearly depends on the ionic strength of the pore solution. Even at the highest ionic
262 strengths value the effective tortuosity is still higher than that of HTO. It can further be observed
263 that the effective tortuosity for both HTO and $^{36}\text{Cl}^-$ is higher in the case of the Helvetic Marl
264 sample than in the case of the Opalinus Clay sample. The pathways in Helvetic Marl sample
265 are thus more tortuous than those in Opalinus Clay sample, and the pathway of $^{36}\text{Cl}^-$ is more
266 tortuous than that of HTO.

267 The tortuosity depends strongly on the mineral composition of the rock and on the arrangement
268 of the composing particles. In the case of Opalinus Clay sample, the clay mineral content is 69
269 wt.%. The majority of the non-clay minerals are quartz (20 wt.%) and calcite (6 wt.%). In the
270 case of Helvetic Marl sample, the situation is different. The non-clay mineral amount is with
271 74 wt.% more than twice as high as in Opalinus Clay sample. Opalinus Clay sample can thus
272 be seen as a clay matrix with some dispersed non-clay mineral grains whereas the Helvetic Marl
273 sample is predominantly a non-clay matrix with clay minerals in between the grains. This
274 potential microstructure for both Opalinus Clay and Helvetic Marl rock samples is
275 schematically depicted in Figure 4.

276 The difference in microstructure and the resulting difference in connectivity/tortuosity of both
277 rocks are mainly caused by their different microstructural framework. In Opalinus Clay, clay

This is a 'pre-publication' version of an accepted article for Clays and Clay Minerals.

This version may be subject to change during the production process.

The DOI given, which may be used for citation purposes, though which will not be active until the version of record is published, is DOI: 10.1346/CCMN.2018.064101

278 minerals dominate and form the structural framework. The connectivity in Opalinus Clay
279 sample is thus mainly dictated by the arrangement of the clay particles and not by the
280 arrangement of the non-clay minerals. In Helvetic Marl sample non-clay minerals build the
281 structural framework and are responsible for the connectivity/tortuosity. Due to the larger
282 degree of compaction, cementation and grain-to-grain contact of the non-clay particles,
283 tortuosity in the Helvetic Marl sample is larger than that in the Opalinus Clay sample (Figure
284 4). Moreover, as soon as non-clay mineral grains squeeze the aligned clay minerals together
285 (Figure 5), a micro-smearing zone occurs (Schmatz *et al.*, 2010; Hemes *et al.*, 2015; Vrolijk *et*
286 *al.*, 2016). That means that the clay minerals are closer together and diffuse double layers
287 overlap in all probability more than in the undisturbed zone (Figure 5). This effect leads to a
288 more frequent occurrence of bottleneck pores in the micro-smearing zone than in the uncrushed
289 zone. The higher probability of the presence of constricted clay mineral texture caused by the
290 movement and realignment of grains through compaction in the Helvetic Marl sample results
291 in more bottleneck pores than in Opalinus Clay sample (Figure 4 and Figure 5). That means
292 that even with less but larger pores, the anion transport is limited due to small pore entries.

293 Wigger and Van Loon (2017) discussed the effect of ionic strength on the transport accessible
294 porosities of anions in the framework of the electrostatic properties of the porous media. At
295 lower ionic strength of the pore water the extent of the electric double layer on the walls of
296 charged pores is thicker than at high ionic strength (Moors, 2005), resulting in a decreased
297 accessible porosity for anions. Not only the accessible porosity, but also the effective tortuosity
298 might be subject to such electrostatic effects. Overlapping of electric double layers might act
299 as barriers for anions. The more barriers there are, the more detours are needed for anions
300 diffusing through an argillaceous rock (Figure 5). Hence, with lower ionic strength not only the
301 accessible porosity for anions is smaller, but also direct transport paths are limited by
302 overlapping electric double layers. As a result, anions have to diffuse along a longer path

303 compared to the clay thickness, *i.e.* the effective tortuosity is larger (Table 4). This also explains
304 the dependency of the effective tortuosity of anion diffusion on ionic strength and the
305 independency of that of the uncharged HTO, which is not limited by overlapping diffuse double
306 layers (Figure 3). The effective tortuosity in the case of diffusion of $^{36}\text{Cl}^-$ in Helvetic Marl
307 sample seems to decrease faster with increasing porosity than that in Opalinus Clay sample
308 (Figure 6). Thus, the anion diffusion behavior in the Opalinus Clay sample is less sensitive to
309 the change of electric double layer thickness, supporting the assumption that the geometry of
310 the matrix is influencing the anion diffusion and, in this case, it is indicated that the Helvetic
311 Marl rock sample has more narrower pore openings (*i.e.* bottleneck-like pores) than the
312 Opalinus Clay rock sample.

313

314 **Data analysis of bottleneck effect with mercury intrusion porosimetry**

315 Both the hysteresis displayed by withdrawal and reinjection curves, and the early breakpoint of
316 the extrusion curve (Figure 2), indicate that both rock samples have a retention potential. Clay
317 rocks exhibit a pore network with different pore sizes, which are randomly arranged. As the
318 pressure falls below the threshold for a given size, individual pores empty sequentially in the
319 order of increasing size. Wardlaw and McKellar (1981) discussed a model in which isolated
320 clusters of large elements occurred in a continuous network of smaller elements. Based on this
321 insight it is assumed that, if clay samples are completely filled with mercury and then the
322 pressure is decreased, the mercury first withdraws from the smallest pores and next withdraws
323 progressively with increasing pore size (Wardlaw and Cassan, 1979). However, in the case of
324 large pores connected by small pores extensive residual mercury is retained, because at the
325 stage where pressure has been reduced below the threshold for emptying of clusters of these
326 large pores, they have already become disconnected by “snap-off” (Figure 7).

327 Due to the snap-off effect bottleneck pores remain filled with mercury. The whole process is
328 observed by the pressure to pore size function (equation 9), and the hysteresis helps to quantify
329 the amount of mercury that withdraws from the bottleneck pores. From the amount of
330 withdrawn mercury obtained from the difference of total volume intruded between the 1st and
331 2nd Hg-intrusion measurements, the volume of the bottleneck pores can be calculated which
332 results in 61.5% for Opalinus Clay and 76.8% for Helvetic Marl, respectively. Also, the visual
333 analysis of the hysteresis curves indicates a more distinct hysteresis effect of the Helvetic Marl
334 sample than the one of Opalinus Clay. This shows very plainly that Helvetic Marl rock sample
335 has a larger bottleneck pore volume than Opalinus Clay rock sample. The analysis at pore scale
336 > 3 nm could give an indication about the pore structure at the micropore scale.

337

338

CONCLUSION

339 The goal of this work was to analyze the pore geometry of Opalinus Clay and Helvetic Marl
340 rock samples, hereby specifically addressing the occurrence of so-called bottleneck pores and
341 its influence on the anion transport. Bottleneck pores limit the anion diffusion independent of
342 the pore size and independent of the ionic strength. Due to the narrow openings of these pores
343 the electric double layers in the pore throat overlap. Consequently, bottleneck pores behave
344 similarly to interlayer pores and hinder anion transport in argillaceous rocks. In order to
345 investigate the amount of bottleneck pores two different methods were used in this study:
346 effective tortuosity calculations and Hg-retention potential measurements. A pore network
347 result from squashed platelets has more bottleneck pores and causes a larger effective tortuosity.
348 The results of this investigation show that Opalinus Clay sample has a smaller effective
349 tortuosity than Helvetic Marl sample. This could be observed both for the neutral tracer HTO
350 as well as for the anionic tracer $^{36}\text{Cl}^-$. Additionally, independent mercury intrusion and extrusion
351 porosimetry measurements performed in this study support the conclusion of a larger Hg-
352 retention potential for Helvetic Marl sample than for Opalinus Clay sample by visual analysis
353 of the hysteresis effect and by analyzing the residual volume data. The fact that the Helvetic
354 Marl sample has a larger Hg-retention potential than the Opalinus Clay sample corroborates the
355 assumption that the Helvetic Marl sample has more bottleneck pores than the Opalinus Clay
356 sample, which seems to influence in the effective tortuosity and the anion diffusion.

357

358

ACKNOWLEDGEMENTS

359 The authors would like to thank A. Röthlisberger for assistance during the experimental work
360 at the Claylab ETH, Switzerland. The authors also wish to thank L. Kennell-Morrison, who
361 reviewed the manuscript from an English grammar perspective. This study was partially
362 financed by the Nuclear Waste Management Organization of Canada (NWMO) and the Paul
363 Scherrer Institut (PSI).

364

- 366 Altmann, S. (2008) Geochemical research: A key building block for nuclear waste disposal
367 safety cases. *Journal of Contaminant Hydrology*, **102**(3), 174-179.
- 368 Appelt, H., Holtzclaw, K. and Pratt, P. (1975) Effect of anion exclusion on the movement of
369 chloride through soils. *Soil Science Society of America Journal*, **39**(2), 264-267.
- 370 Baeyens, B. and Bradbury, M. H. (2004) Cation exchange capacity measurements on illite using
371 the sodium and cesium isotope dilution technique: effects of the index cation, electrolyte
372 concentration and competition: modeling. *Clays and Clay Minerals*, **52**(4), 421-431.
- 373 Bolt, G. H. and de Haan, F. A. M. (1979) Chapter 7: Anion exclusion in soil. *Developments in*
374 *Soil Science*. Elsevier. **5**(B), 233-257.
- 375 Chagneau, A. L., Tournassat, C., Steefel, C. I., Bourg, I. C., Gaboreau, S.P., Esteve, I. N.,
376 Kupcik, T., Claret, F., and Schäfer, T. (2015) Complete restriction of $^{36}\text{Cl}^-$ diffusion by
377 celestite precipitation in densely compacted illite. *Environmental Science & Technology*
378 *Letters*, **2**(5), 139-143.
- 379 Choi, J.-W. and Oscarson, D. (1996) Diffusive transport through compacted Na-and Ca-
380 bentonite. *Journal of Contaminant Hydrology*, **22**(3), 189-202.
- 381 Descostes, M., Blin, V., Bazer-Bachi, F., Meier, P., Grenut, B., Radwan, J., Schlegel, M. L.,
382 Buschaert, S., Coelho, D., and Tevissen, E. (2008) Diffusion of anionic species in
383 Callovo-Oxfordian argillites and Oxfordian limestones (Meuse/Haute-Marne, France).
384 *Applied Geochemistry*, **23**(4), 655-677.
- 385 Diamond, S. (1970) Pore size distributions in clays. *Clays and clay minerals*, **18**(1), 7-23.
- 386 Flury, M. and Gimmi, T. F. (2002) 6.2 Solute diffusion. *Methods of Soil Analysis: Part 4*, 1323-
387 1351.
- 388 Gaboreau, S., Robinet, J.C. and Prêt, D. (2016) Optimization of pore-network characterization
389 of a compacted Clay material by TEM and FIB/SEM imaging. *Microporous and*
390 *Mesoporous Materials* **224**, 116-128.
- 391 Giesche, H. (2006) Mercury porosimetry: a general (practical) overview. *Particle & particle*
392 *systems characterization*, **23**(1), 9-19.
- 393 Gimmi, T. and Fernández, A.M. (2017). Physical characterisation of pores and pore water of
394 samples from the Schlattingen borehole. *Technical Report NAB 16-71*. Nagra,
395 Wettingen, Switzerland.
- 396 Grambow, B. (2008) Mobile fission and activation products in nuclear waste disposal. *Journal*
397 *of Contaminant Hydrology*, **102**(3), 180-186.
- 398 Harvey, K. B. (1996) Measurement of diffusive properties of intact rock, Atomic Energy of
399 Canada Ltd.
- 400 Hemes, S., Desbois, G., Urai, J. L., Schröppel, B., and Schwarz, J.-O. (2015) Multi-scale
401 characterization of porosity in Boom Clay (HADES-level, Mol, Belgium) using a
402 combination of X-ray μ -CT, 2D BIB-SEM and FIB-SEM tomography. *Microporous*
403 *and mesoporous materials*, **208**, 1-20.
- 404 Houben, M., Desbois, G., and Urai, J. L. (2013) Pore morphology and distribution in the shaly
405 facies of Opalinus Clay (Mont Terri, Switzerland): Insights from representative 2D
406 BIB-SEM investigations on mm to nm scale. *Applied Clay Science*, **71**, 82-97.
- 407 Katsube, T., Melnyk, T., and J. Hume (1986) *Pore structure from diffusion in granitic rocks*,
408 Atomic Energy of Canada Limited, Whiteshell Nuclear Research Establishment.
- 409 Kestin, J., Khalifa, H. E., and Correia, R. J. (1981) Tables of the dynamic and kinematic
410 viscosity of aqueous NaCl solutions in the temperature range 20–150 C and the pressure
411 range 0.1–35 MPa. *Journal of physical and chemical reference data*, **10**(1), 71-88.

- 412 Matuszewick, M., Pirkkalainen, K., Liljeström, V., Suuronen, J.P., Root, A., Muurinen, A.,
413 Serimaa, R. and Olin, M. (2013). Microstructural investigation of calcium
414 montmorillonite. *Clay Minerals*, **48**, 267-276.
- 415 Mazurek, M., Waber, N., Mäder, U., Gimmi, T., de Haller, A., and Koroleva, M. (2012)
416 Geochemical synthesis for the Effingen Member in boreholes at Oftringen, Gösigen and
417 Küttigen. *Technical Report NTB 12-07*. Nagra, Wettingen, Switzerland.
- 418 Melnyk, T. and Skeet, A. (1986) An improved technique for the determination of rock porosity.
419 *Canadian Journal of Earth Sciences*, **23**(8), 1068-1074.
- 420 Moors, H. (2005) Topical report on the effect of the ionic strength on the diffusion accessible
421 porosity of Boom Clay. *SCK CEN, Mol, Belgium, report SCK A CEN-ER-02*.
- 422 Moro, F. and Böhni, H. (2002) Ink-bottle effect in mercury intrusion porosimetry of cement-
423 based materials. *Journal of Colloid and Interface Science*, **246**(1), 135-149.
- 424 Muurinen, A. (1994) Diffusion of anions and cations in compacted sodium bentonite. *VTT*
425 *Publications 168*, Technical Research Centre of Finland, Espoo, Finland.
- 426 Schmatz, J., Vrolijk, P., and Urai, J. (2010) Clay smear in normal fault zones—The effect of
427 multilayers and clay cementation in water-saturated model experiments. *Journal of*
428 *Structural Geology*, **32**(11), 1834-1849.
- 429 Smith, D., Pivonka, P., Jungnickel, C., and Fityus, S. (2004) Theoretical analysis of anion
430 exclusion and diffusive transport through platy-clay soils. *Transport in porous media*,
431 **57**(3), 251-277.
- 432 Song, Y., Davy, C. A., Bertier, P., and Troadec, D. (2016) Understanding fluid transport
433 through claystones from their 3D nanoscopic pore network. *Microporous and*
434 *Mesoporous Materials*, **228**, 64-85.
- 435 Tevissen, E., Soler, J., Montarnal, P., Gautschi, A., and L. R. Van Loon (2004) Comparison
436 between in situ and laboratory diffusion studies of HTO and halides in Opalinus Clay
437 from the Mont Terri. *Radiochimica Acta/International journal for chemical aspects of*
438 *nuclear science and technology*, **92**(9-11/2004), 781-786.
- 439 Thompson, M. L., McBride, J. F., and Horton, R. (1985) Effects of drying treatments on
440 porosity of soil materials. *Soil science society of America journal*, **49**(6), 1360-1364.
- 441 Tournassat, C. and Appelo, C. A. J. (2011) Modelling approaches for anion-exclusion in
442 compacted Na-bentonite. *Geochimica et Cosmochimica Acta*, **75**(13), 3698-3710.
- 443 Tournassat, C., Bourg, I. C., Holmboe, M., Sposito, G., and Steefel, C. I. (2016a) Molecular
444 dynamics simulations of anion exclusion in clay interlayer nanopores. *Clays and Clay*
445 *Minerals*, **64**(4), 374-388.
- 446 Tournassat, C., Gaboreau, S., Robinet, J.-C., Bourg, I. C., and Steefel, C. I. (2016b) Impact of
447 microstructure on anion exclusion in compacted clay media. *The Clay Mineral Society*
448 *Workshop Lectures Series*. **21, Chapter 11**, 137-149.
- 449 Van Brakel, J. and Heertjes, P. M. (1974) Analysis of diffusion in macroporous media in terms
450 of a porosity, a tortuosity and a constrictivity factor. *International Journal of Heat and*
451 *Mass Transfer*, **17**(9), 1093-1103.
- 452 Van Loon, L. R., Glaus, M. A., and Müller, W. (2007) Anion exclusion effects in compacted
453 bentonites: Towards a better understanding of anion diffusion. *Applied Geochemistry*,
454 **22**(11), 2536-2552.
- 455 Van Loon, L. R. and Soler, J. M. (2004) Diffusion of HTO, ³⁶Cl⁻, ¹²⁵I⁻ and ²²Na⁺ in Opalinus
456 Clay: Effect of Confining Pressure, Sample Orientation, Sample Depth and
457 Temperature. *Nagra Technischer Bericht NTB 03-07*. Nagra, Wettingen, Switzerland,
458 Paul-Scherrer-Institut, PSI.
- 459 Vilks, P. and Miller, N. (2007) Evaluation of experimental protocols for characterizing
460 diffusion in sedimentary rocks. *Nuclear Waste Management Organization Report TR-*
461 *2007-11*. Nuclear Waste Management Organization, Toronto, Canada.

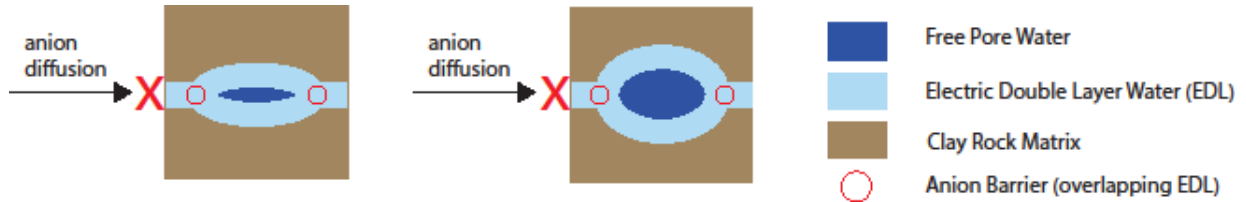
462 Vrolijk, P. J., Urai, J. L., and Kettermann, M. (2016) Clay smear: Review of mechanisms and
463 applications. *Journal of Structural Geology*, **86**, 95-152.
464 Wardlaw, N. and Cassan, J. (1979) Oil recovery efficiency and the rock-pore properties of some
465 sandstone reservoirs. *Bulletin of Canadian Petroleum Geology*, **27**(2), 117-138.
466 Wardlaw, N. and McKellar, M. (1981) Mercury porosimetry and the interpretation of pore
467 geometry in sedimentary rocks and artificial models. *Powder technology*, **29**(1), 127-
468 143.
469 Washburn, E. W. (1921a) The dynamics of capillary flow. *Physical review*, **17**(3), 273.
470 Washburn, E. W. (1921b) Note on a method of determining the distribution of pore sizes in a
471 porous material. *Proceedings of the National Academy of Sciences*, **7**(4), 115-116.
472 Wigger, C., Gimmi, T., Muller, A. C. A., and Van Loon, L. R. (2018) The influence of small
473 pores on the anion transport properties of natural argillaceous rocks – a pore size
474 distribution investigation of Opalinus Clay and Helvetic Marl. *Applied Clay Science*,
475 **156**, 134-143.
476 Wigger, C. and Van Loon, L. R. (2017) Importance of interlayer equivalent pores for anion
477 diffusion in clay-rich sedimentary rocks. *Environmental Science & Technology*, **51**(4),
478 1998-2006.
479
480

481

Figures

482

483



484

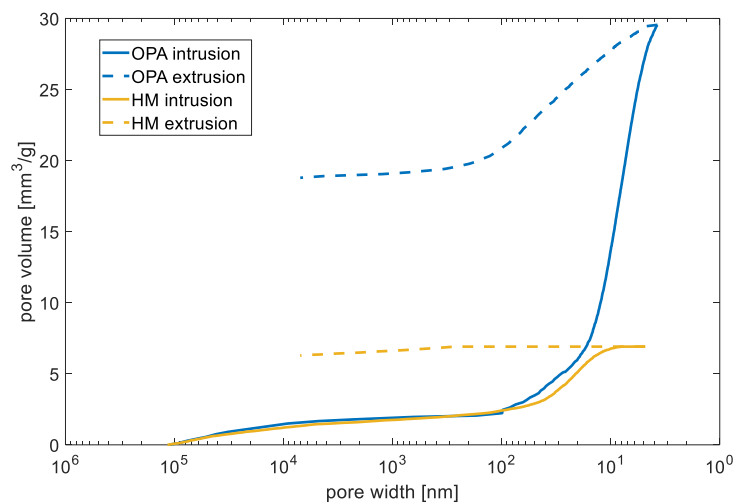
485

Figure 1 Schematic view of bottleneck pores in argillaceous rocks with overlapping electric double layers at the pore opening independent on the pore size.

486

487

488



489

Figure 2 Intrusion and extrusion curves of a mercury intrusion porosimetry measurement for Opalinus Clay (OPA) and Helvetic Marl (HM) samples. (pore width = pore diameter)

490

491

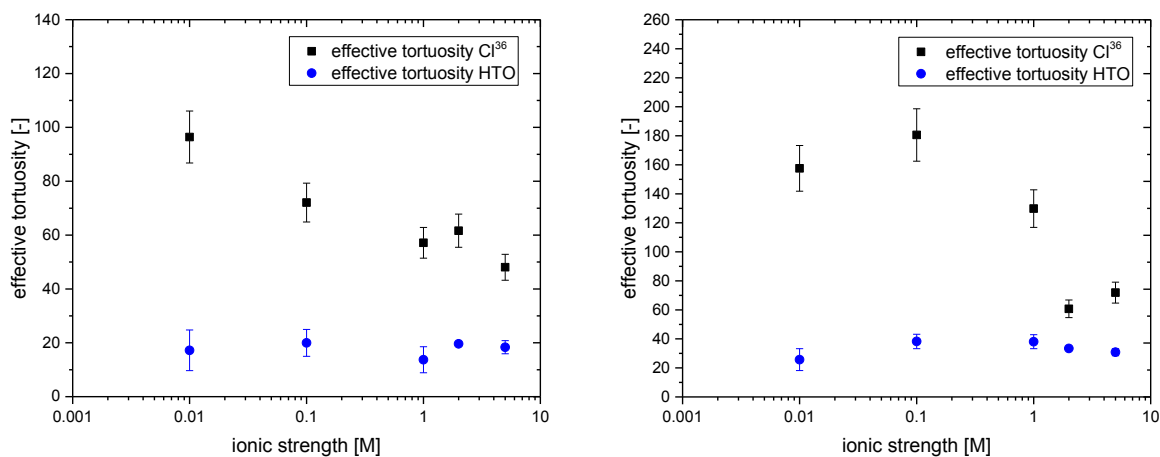
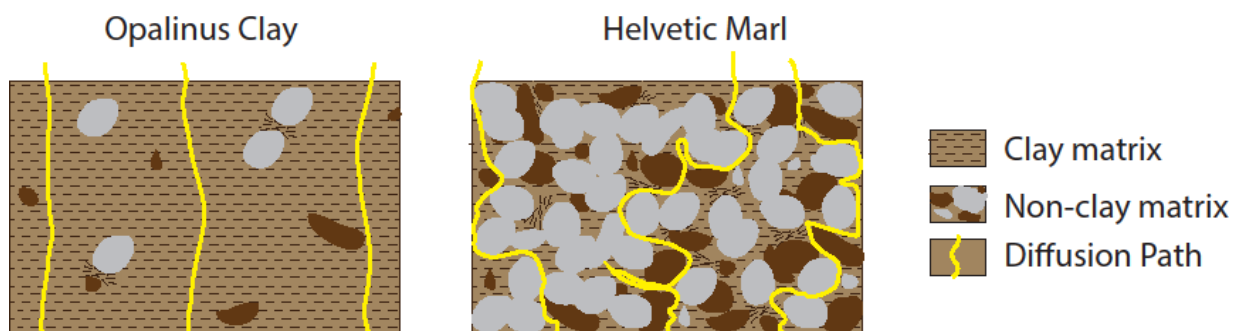


Figure 3 Effective tortuosity for the diffusion of HTO and ³⁶Cl⁻ in Opalinus Clay (left) and Helvetic Marl (right) samples as a function of the chemical composition of the pore water.

492

493

494

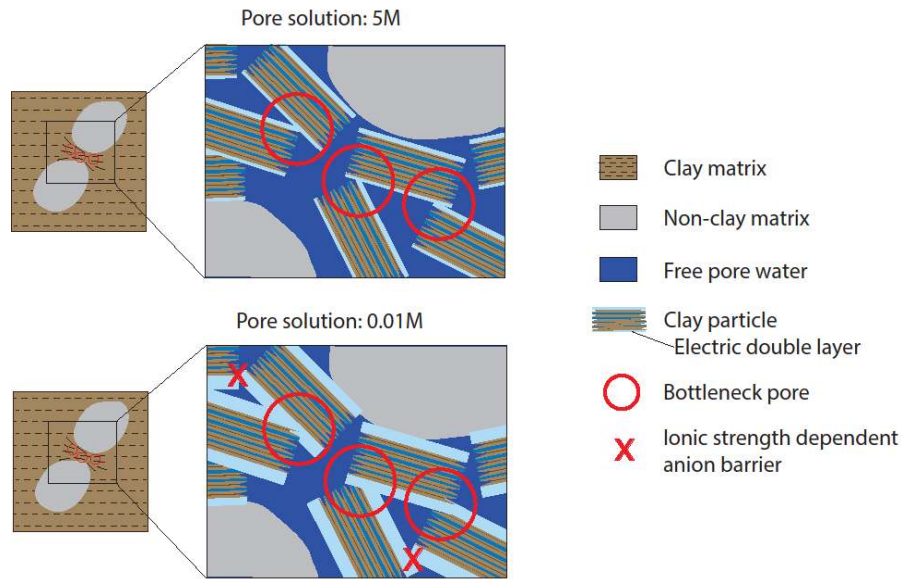


495

496

Figure 4 Cartoon picture of the microstructure and expected connectivity for Opalinus Clay and Helvetic Marl samples.

497

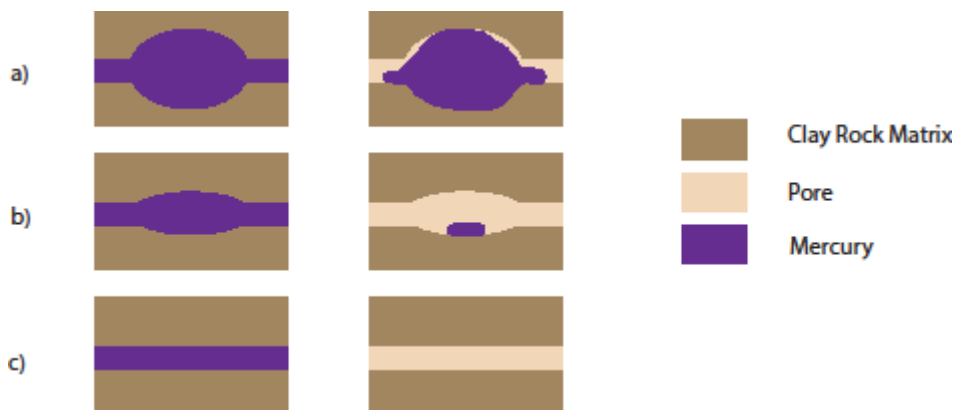


498

Figure 5 The lower the ionic strength of the pore water; the thicker are the electric double layers. Hence, there are more overlapping electric double layers acting as barriers and the anions have longer transport paths through the clay. This is more distinct in pore networks with narrow pore openings, like in the Helvetic Marl rock sample.

499

500



501

Figure 7 Schematic view of trapped mercury in argillaceous rock pores before and after pressure reduction. a) Pore with a large pore to throat size ratio [> 3] b) pore with a smaller pore to throat size ratio [> 1] c) pore with a small pore to throat size ratio [≤ 1]. (After Wardlaw and McKellar, 1981)

502

503

504

505

Tables

Table 1 Mineralogical composition and physico-chemical properties of Opalinus Clay and Helvetic Marl rock samples used in this work (from Wigger and Van Loon, 2017).

Parameters	Opalinus Clay	Helvetic Marl
Sample	SLA - 936.25	WLB SB4a/v -475.86
Grain density (kg/dm ³)	2.70 ± 0.002	2.73 ± 0.001
Bulk dry density (kg/dm ³)	2.46 ± 0.03	2.66 ± 0.03
¹ Total porosity (%)	8.9 ± 1	2.6 ± 1
² Mode pore size (nm)	7	20
³ CEC (meq/kg sample)	105 ± 0.5	56 ± 0.2
⁴Mineralogy (wt.%)		
Non phyllosilicates (wt.%)	31 ± 3	74 ± 3
Calcite	6	38
Dolomite/Ankerite	< 1	7
Siderite	2	0
Na-Plagioclase	1	2
K-Feldspar	2	1
Pyrite	< 1	1
Quartz	20	25
Phyllosilicates (wt.%)	69 ± 3	26 ± 3
Kaolinite	28	< 1
Illite	25	11
Illite-smectite	8	4
Chlorite	8	11

506 ¹calculated from the grain and bulk dry density

507 ²defined with mercury intrusion porosimetry measurements

508 ³measured by the Cs-method (Baeyens and Bradbury 2004)

509 ⁴analyzed as described in Mazurek *et al.* (2012)

510

Table 2 Summary of effective diffusion coefficients D_e , diffusion coefficients of pore water solution D_{ps} and porosity values η_t obtained for Opalinus Clay and Helvetic Marl rock samples to calculate the effective tortuosity τ_D^2 for diffusion in argillaceous rocks with 1 M NaCl pore water.

		HTO		³⁶ Cl ⁻	
		Opalinus Clay sample	Helvetic Marl sample	Opalinus Clay sample	Helvetic Marl sample
¹ η_t	[-]	0.114	0.03	0.069	0.0085
D_{ps}	[m ² s ⁻¹]	1.85·10 ⁻⁹		1.85·10 ⁻⁹	
¹ D_e	[m ² s ⁻¹]	1.12·10 ⁻¹¹	1.06·10 ⁻¹²	2.25·10 ⁻¹²	1.22·10 ⁻¹³
τ_D^2	[-]	1.88·10¹	5.24·10¹	5.67·10¹	1.29·10²

¹Values are from Wigger and Van Loon (2017)

511

Table 3 Mercury intrusion volume data of Opalinus Clay and Helvetic Marl samples.

Opalinus Clay				Helvetic Marl			
	[mm ³ /g]	[%]	¹ [%]		[mm ³ /g]	[%]	¹ [%]
1 st run ²				1 st run			
total vol. (V _{tot})	29.6	100		total vol. (V _{tot})	6.9	100	
withdraw vol. (V_w)	10.8	36		withdraw vol. (V_w)	0.6	9	
trapped vol. ³	18.8	64		trapped vol.	6.3	91	
2 nd run				2 nd run			
total vol. (V _{tot})	11.4	100	39	total vol. (V _{tot})	1.6	100	23
withdraw vol. (V _w)	10.6	93		withdraw vol. (V _w)	1.2	74	
trapped vol. ³	0.8	7		trapped vol.	0.4	26	

512

¹ from Wigger and Van Loon (2017)

513

² 1st run: first intrusion-extrusion cycle; 2nd run: second intrusion-extrusion cycle;

514

³ trapped vol.: difference of Hg volume from intrusion and extrusion curves;

515

516

Table 4 Summary of porosities η_t obtained by diffusion experiments (Wigger and Van Loon, 2017) and calculated effective tortuosity values τ_D^2 for Opalinus Clay and Helvetic Marl samples with varying ionic strength I of the pore water (NaCl).

I [M]	³⁶ Cl ⁻ Helvetic Marl sample		Opalinus Clay sample	
	η_t	τ_D^2	η_t	τ_D^2
0.01	0.0055	157.54	0.03	96.43
0.1	0.0078	180.57	0.043	72.09
1	0.0085	129.81	0.069	57.14
2	0.0078	60.73	0.074	61.62
5	0.0110	71.91	0.084	48.05

517

518

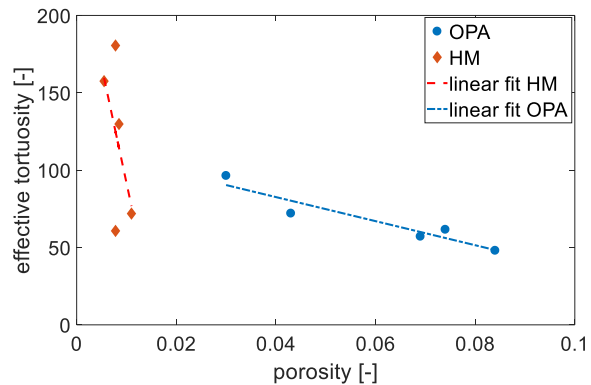
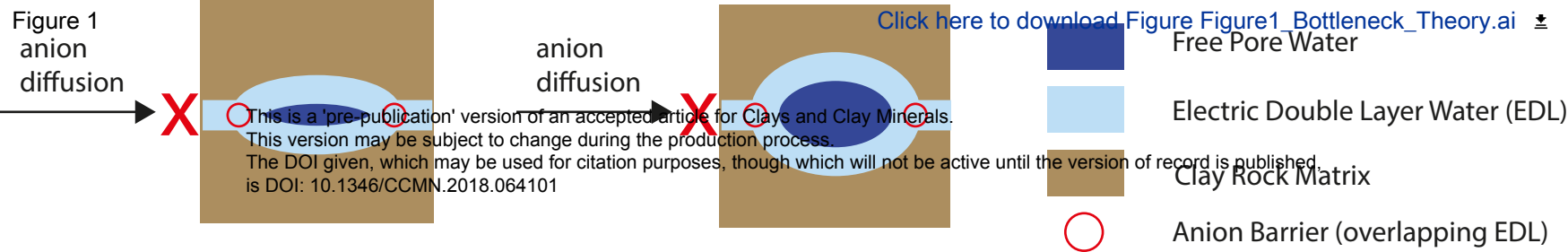
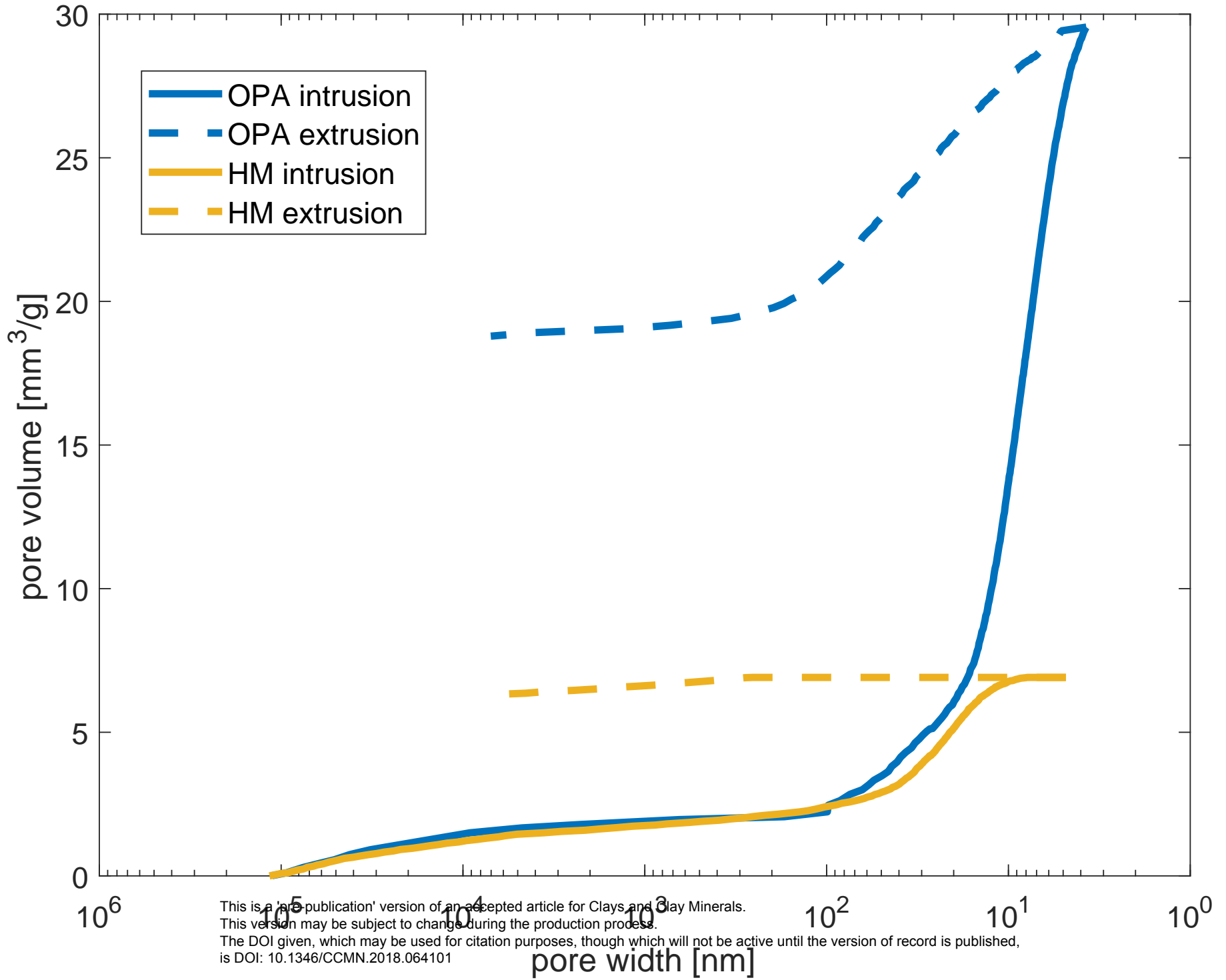
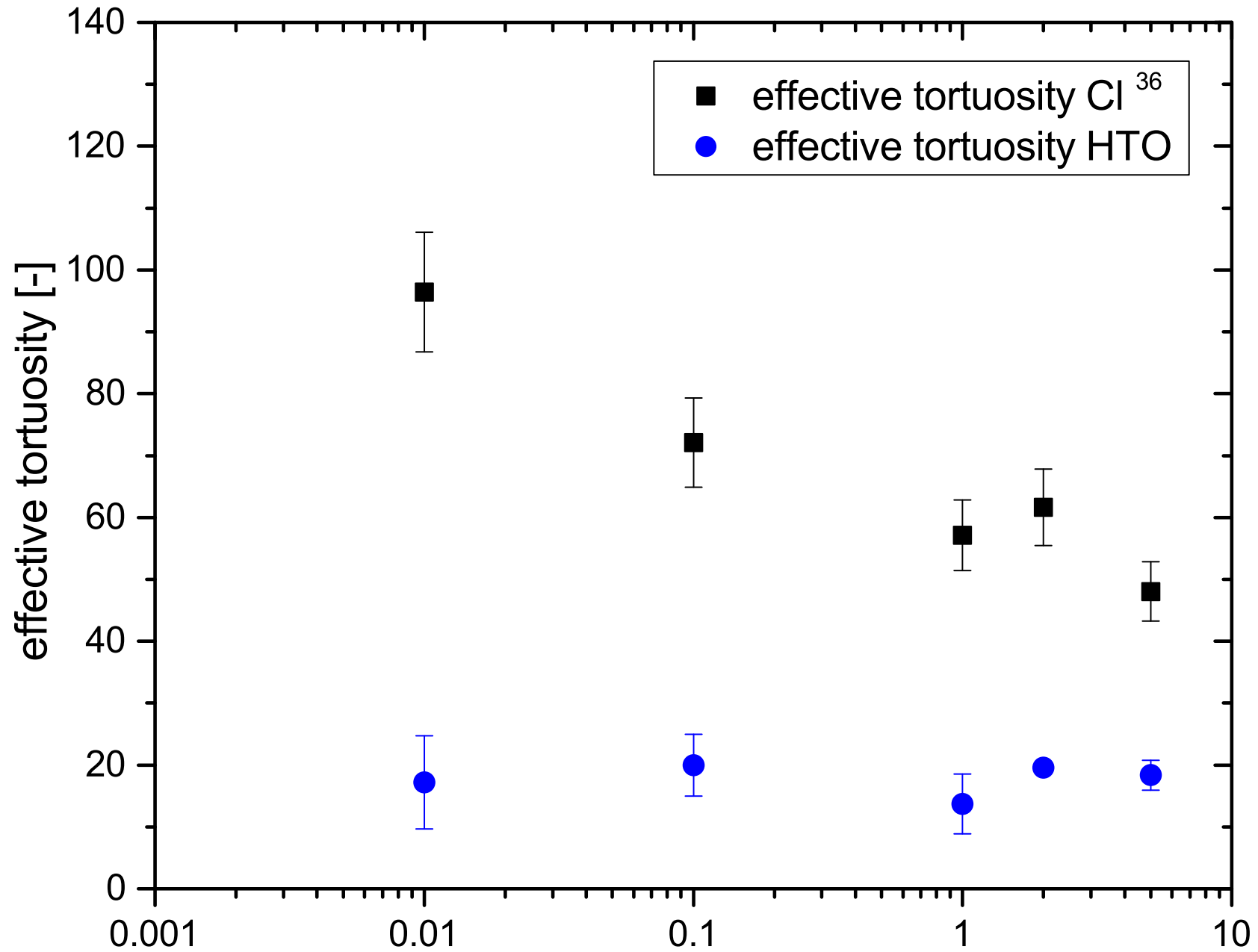


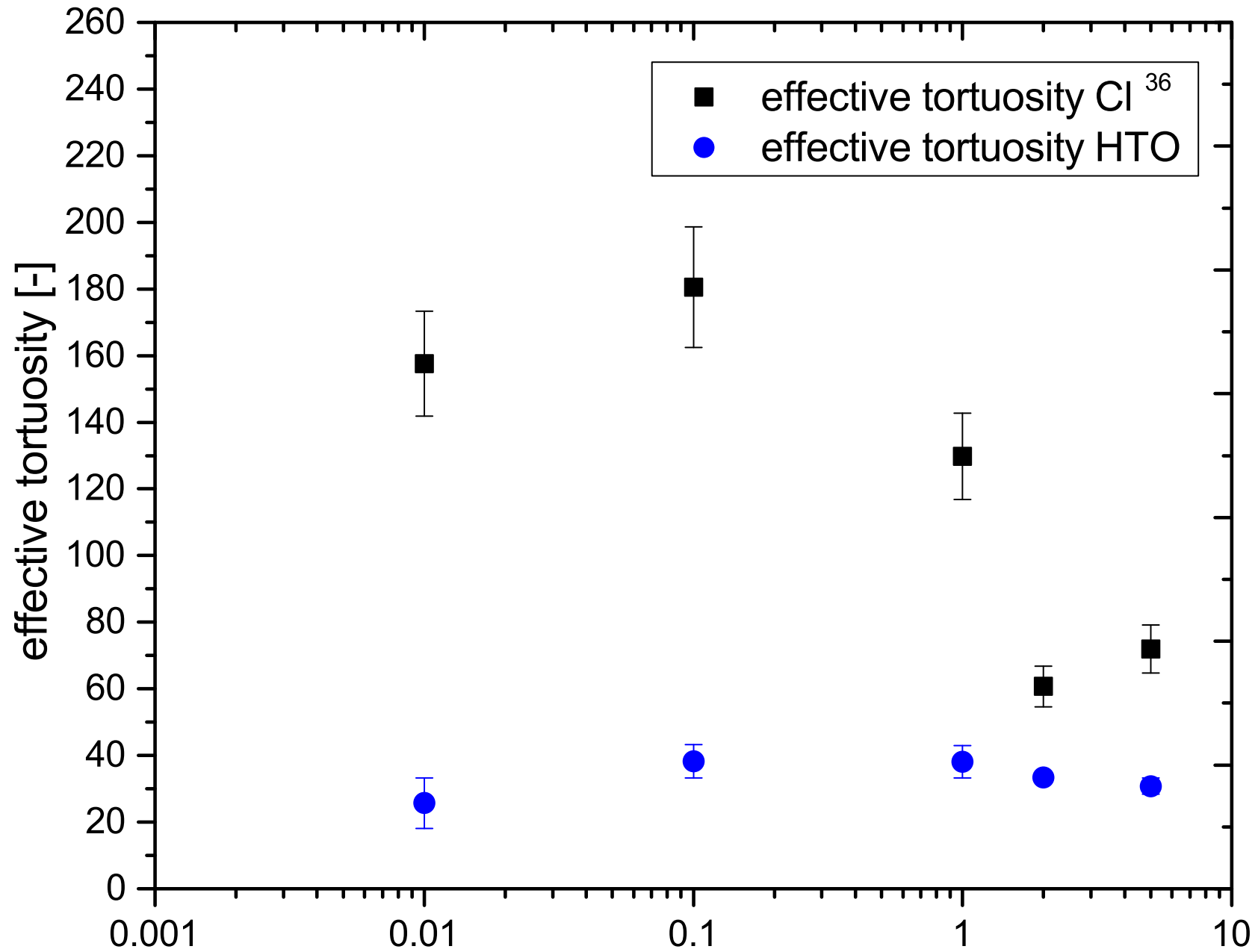
Figure 6 Effective tortuosity values of ³⁶Cl⁻ Helvetic Marl and Opalinus Clay samples plotted against the respective porosity.





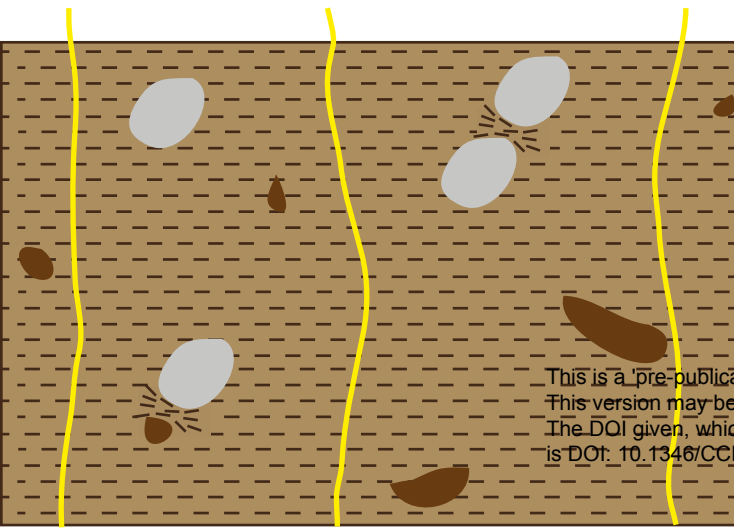
This is a pre-publication version of an accepted article for Clays and Clay Minerals. This version may be subject to change during the production process. The DOI given, which may be used for citation purposes, though which will not be active until the version of record is published, is DOI: 10.1346/CCMN.2018.064101



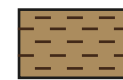
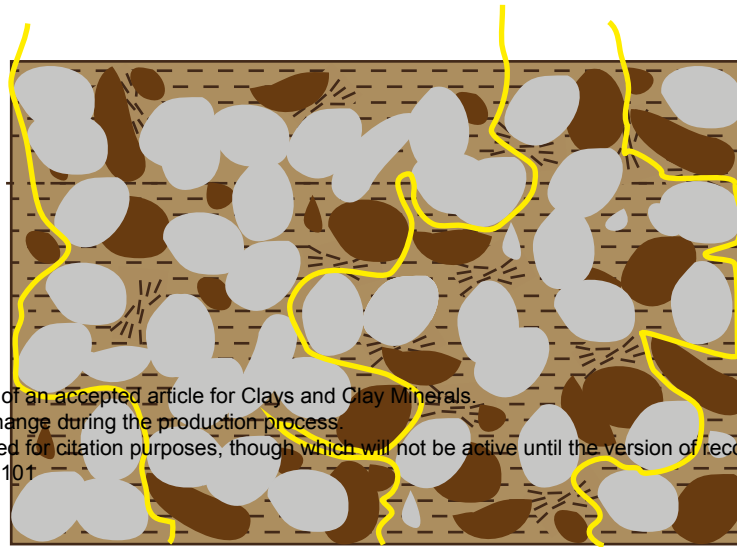


This is a 'pre-publication' version of an accepted article for Clays and Clay Minerals.
This version may be subject to change during the production process.
The DOI given, which may be used for citation purposes, though which will not be active until the version of record is published,
is DOI: 10.1346/CCMN.2018.064101

Opalinus Clay



Helvetic Marl

[Click here to download Figure Figure4_Structure_OPAvsHM.ai](#)

Clay matrix



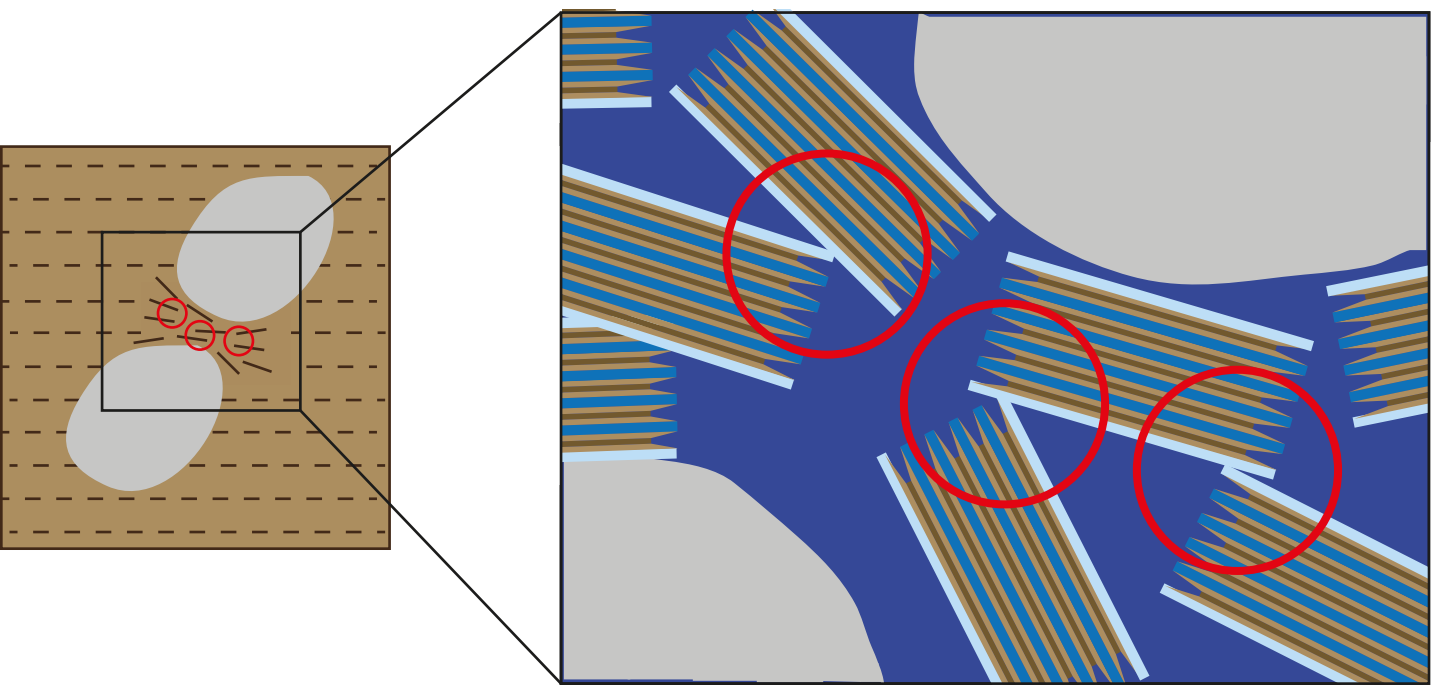
Non-clay matrix



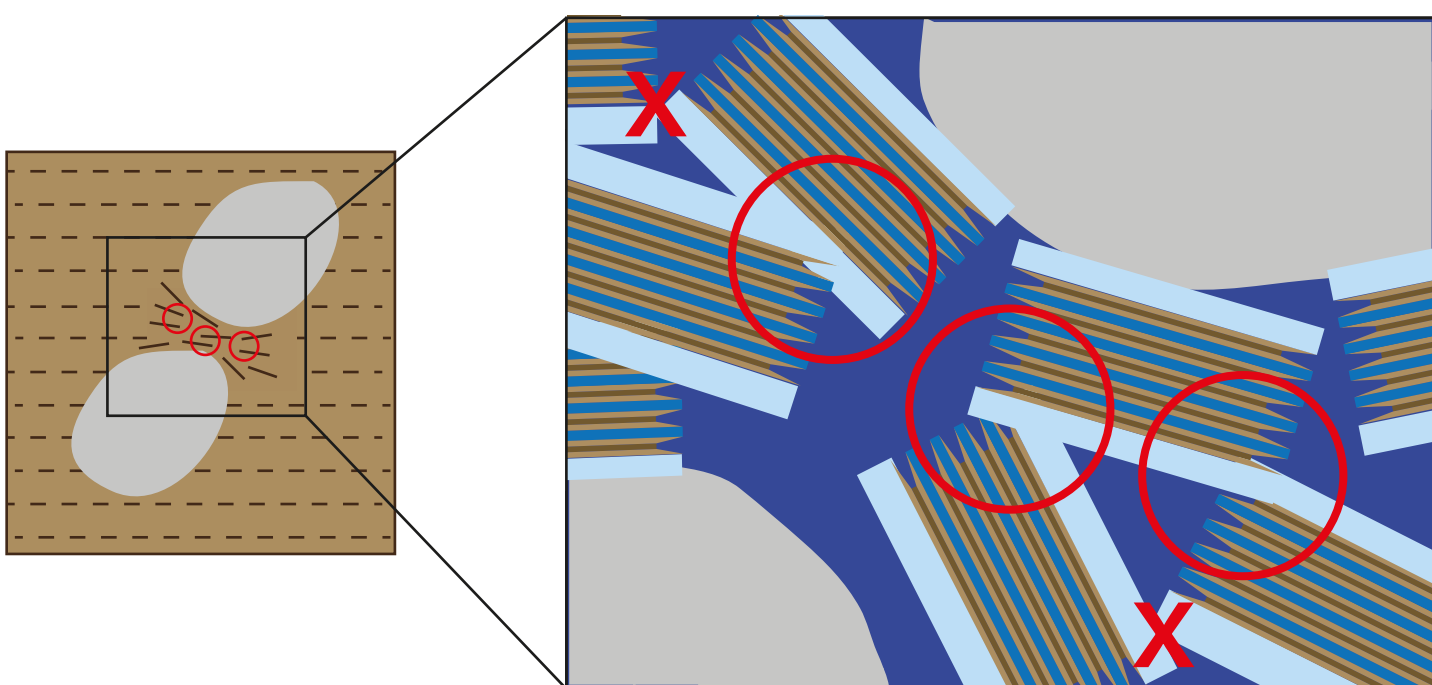
Diffusion Path

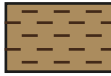



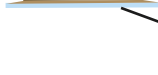


This is a 'pre-publication' version of an accepted article for Clays and Clay Minerals.
This version may be subject to change during the production process.
The DOI given, which may be used for citation purposes, though which will not be active until the version of record is published,
is DOI: 10.1346/CCMN.2018.064101

Pore solution: 5M



Pore solution: 0.01M



-  Clay matrix
-  Non-clay matrix
-  Free pore water
-  Clay particle
-  Electric double layer
-  Bottleneck pore
-  Ionic strength dependent anion barrier

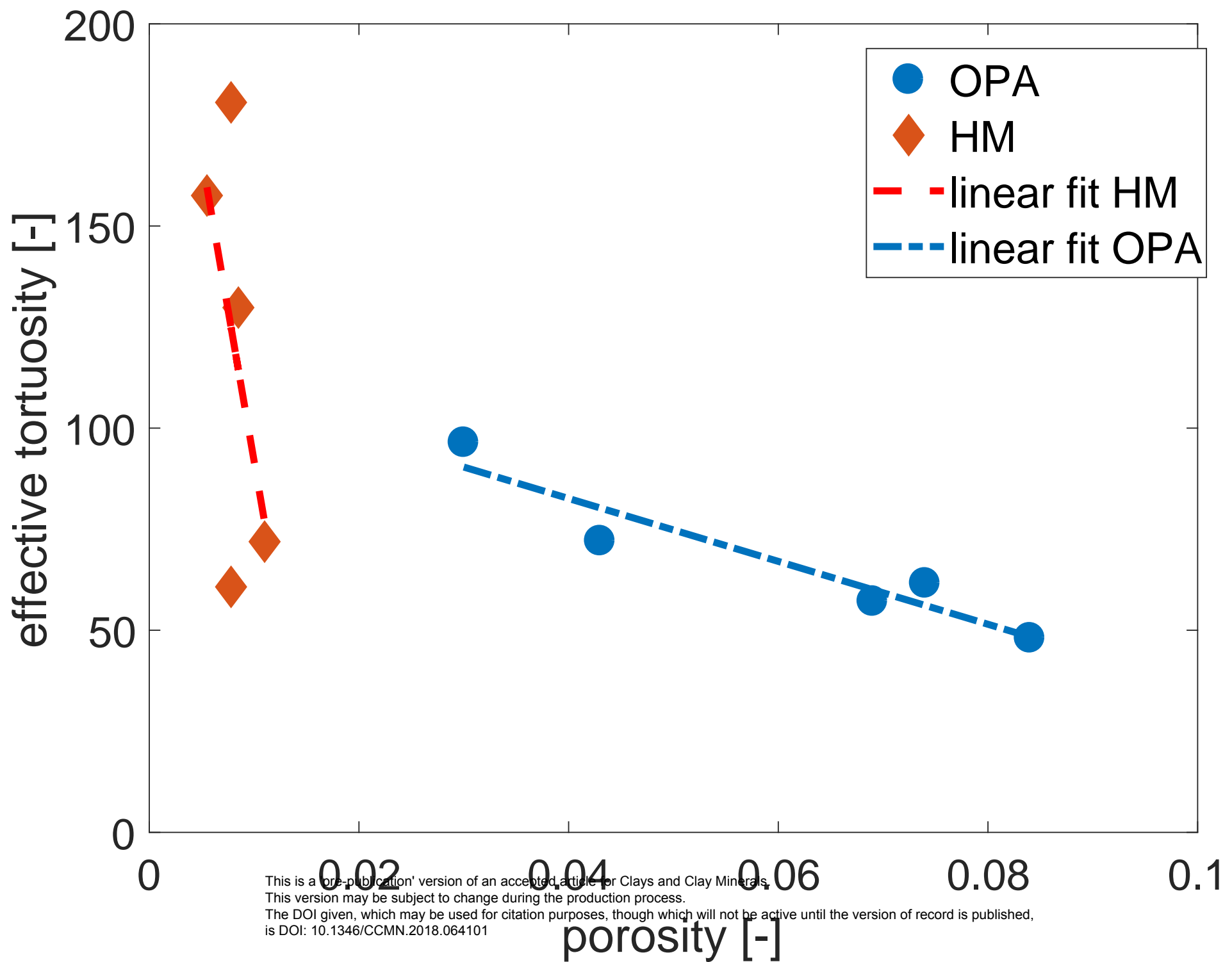
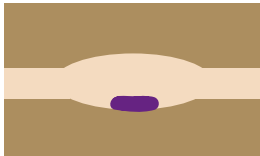
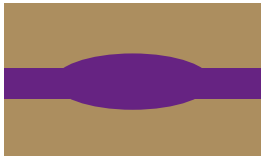


Figure 7

a)



b)



[Click here to download Figure Figure7_MIP_drapping.ai](#)



Clay Rock Matrix



Pore



Mercury

This is a 'pre-publication' version of an accepted article for Clays and Clay Minerals.

This version may be subject to change during the production process.

The DOI given, which may be used for citation purposes, though which will not be active until the version of record is published,

c) is DOI: 10.1346/CCMN.2018.064101